ADVANCED OPTICAL MATERIALS
www.advopticalmat.de

Polarization Reflector/Color Filter at Visible Frequencies via Anisotropic α-MoO_3

Chenwei Wei, Sina Abedini Dereshgi, Xianglian Song, Akshay Murthy, Vinayak P. Dravid, Tun Cao, and Koray Aydin**

2D van der Waals materials have attracted increasing attention in recent years due to their exciting physical properties and offer new opportunities for creating devices with enhanced or novel functionalities. In particular, α-MoO_3 is an emerging member of the fast-growing 2D family with strong natural anisotropic optical properties. However, anisotropic optical properties of -MoO_3 in the visible frequency range remain elusive. Here, α-MoO_3 is investigated as an optical material at the visible frequency (450–750 nm), which exhibits a polarization-dependent complex refractive index due to the anisotropic crystal structure. As a proof of concept, polarization-sensitive photonic devices including polarization reflectors and polarization color filters are designed and realized by constructing metal–insulator–metal Fabry–Perot cavities. It is observed that resonance frequencies for designed transmission and reflection filters change up to 25 nm with incident polarization which stems from the polarization-dependent complex refractive indices of α-MoO_3. The largest contrasts are observed for two orthogonal polarization states parallel to the two orthogonal in-plane crystal directions. The approach in this study offers new directions for potential applications in the development of polarization-dependent devices based on 2D van der Waals materials for visible frequencies.

1. Introduction

Anisotropic optical materials offer a platform that opens up new possibilities for diverse polarization-dependent devices, including integrated digital inverters, artificial synaptic devices, polarization-sensitive photodetectors, mid-infrared polarizers, polarization reflectors, linearly polarized ultrafast lasers, polarization color filters, and polarization sensors, which have been demonstrated with artificial metamaterials.[1–6] However, complexity of existing nanofabrication techniques and the optical losses of metamaterials limit further progress.[7,8]

In recent years, 2D van der Waals (vdW) materials, the layered crystals in which individual atomic planes are held together by weak vdW bonds, have drawn increasing attention due to their unique optical properties.[9–13] Since the first isolation of graphene, 2D vdW materials have grown into a large family[14] and now comprise of both high lattice symmetry isotropic materials and anisotropic materials with low lattice symmetry, such as black phosphorus (BP),[6,15–17] gallium telluride (GaTe)[18] and hexagonal boron nitride(hBN).[19,20] Due to the asymmetrical crystal structure in anisotropic 2D vdW materials, they not only possess properties comparable to those of the most studied isotropic graphene,[14,21] such as a large on/off ratio and high mobility, but also exhibit in-plane electrical, optical and thermal anisotropic properties. This in-plane anisotropy leads to richer physics and provides us another degree of freedom for tuning physical properties. In particular, optical anisotropic 2D vdW materials are outstanding candidates for creating novel polarization-dependent devices.[22–25] In comparison with the artificial metamaterials, due to the exciting optical properties of these vdW materials, optical losses are reduced and complex and multi-step lithographic techniques are not needed to construct optically active nanostructures.

α-phase Molybdenum trioxide (α-MoO_3) has drawn considerable attention as an emerging natural 2D vdW material. Recently, Zheng et al. have identified the appearance of hyperbolic phonon polaritons (PhPs)—hybrid quasiparticles with optical photons produced by illuminating polar materials at infrared frequencies—in 2D vdW α-MoO_3.[26] Following further studies of PhPs in α-MoO_3, novel nanophotonic devices on α-MoO_3 have been proposed, such as broadband absorbers, high quality factor polariton resonators and subwavelength steering

C. Wei, S. Abedini Dereshgi, Dr. X. Song, Prof. K. Aydin
Department of Electrical and Computer Engineering
Northwestern University
Evanston, IL 60208, USA
E-mail: aydin@northwestern.edu
C. Wei, Prof. T. Cao
School of Biomedical Engineering
Dalian University of Technology
Dalian 116000, China
E-mail: caotun1806@dlut.edu.cn
A. Murthy, Prof. V. P. Dravid
Department of Materials Science and Engineering
Northwestern University
Evanston, IL 60208, USA
A. Murthy, Prof. V. P. Dravid
International Institute for Nanotechnology
Northwestern University
Evanston, IL 60208, USA
Prof. V. P. Dravid
Northwestern University Atomic and Nanoscale Characterization Experimental (NUANCE) Center
Northwestern University
Evanston, IL 60208, USA
Prof. T. Cao
School of Optoelectronic Engineering and Instrumentation Science
Dalian University of Technology
Dalian 116024, China

DOI: 10.1002/adom.202000088

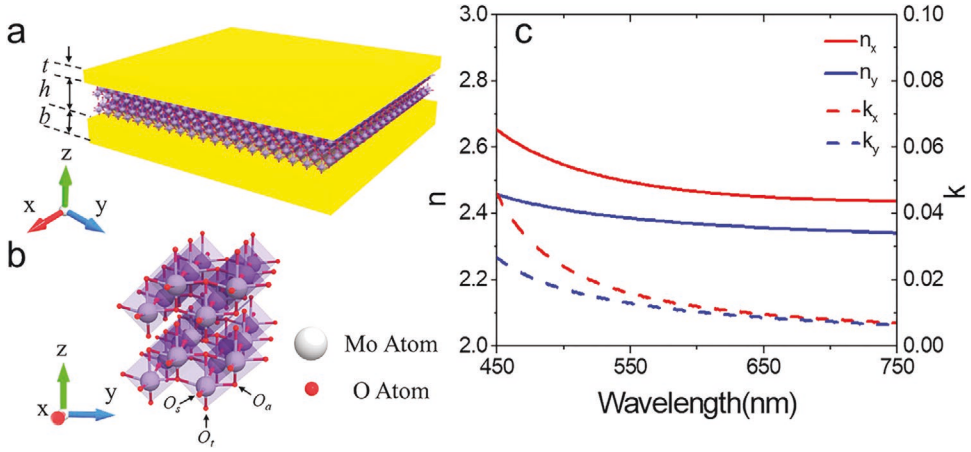

Figure 1. a) Schematic of planar triple-layer metal/α-MoO_3/metal device. b) Illustration of the orthorhombic α-MoO_3 with layered structure held together by van der Waals' forces. c) Real and imaginary parts of the spectral refractive index of α-MoO_3 in the visible range.

and focusing devices.[26–29] However, all the research on α-MoO_3 mentioned above has focused on infrared frequencies, while the characteristics and the application of α-MoO_3 in the visible frequency range have seldom been described.[30] In this work, by designing metal/α-MoO_3/metal Fabry–Perot (FP) cavities, we study the anisotropic optical properties of α-MoO_3 in the visible frequency range. We present the fitting complex refractive index of α-MoO_3. In order to achieve the reflectors and optical filters, α-MoO_3 acts as the insulator in proposed FP cavities. Such a lossless dielectric material with high index contrast can support strong interference effects. Thus, polarization reflectors and color filters via α-MoO_3 are realized, and the calculated spectra match well with experimental results. Optical devices based on α-MoO_3 show polarization-sensitive properties due to the anisotropic crystal structure of α-MoO_3 and the concept can expand to the family of α-MoO_3 materials such as α-MoO_{3-x} and H_xMoO_3[31,32] since they have similar anisotropic crystal structures to α-MoO_3. The proposed optical devices involve only smooth planar surface without complex multi-step lithographic techniques, which enable large area, high throughput, and low cost fabrication. Such polarization-sensitive optical devices could be of use in various potential application areas such as biosensing[33] and photodetectors.[13] Another potential implementation of α-MoO_3 can be in metasurfaces. The recent trend in highly coded dielectric metasurfaces using sub-diffraction arrays has been extremely successful in applying effective medium theory to design devices capable of on-demand phase, amplitude and polarization modulation of light.[34] One of the important directions of research for metasurfaces is to include multiple functionalities coded to the same device, which can be tailored to encoded metasurfaces[35] and counterfeiting technology.[36,37] However, most of the materials used for metasurfaces are isotropic. α-MoO_3 is an inherently anisotropic material which can further increase the design variables (crystal direction) in metasurfaces to enhance encoding capabilities.

2. Results and Discussions

The proposed FP cavity consists of three layers, metal/α-MoO_3/metal, with size parameter of top metal thickness t, middle α-MoO_3 thickness h, and bottom metal thickness b, as shown in **Figure 1**a. As an FP type cavity, multiple round-trip phase shifts of electromagnetic wave inside the resonant cavity is the significant contributory factor[38–40] to the confinement of the wave. The layered α-MoO_3 crystal with its orthorhombic crystal structure composed of bilayer distorted MoO_6 octahedra (Figure 1b) has a highly anisotropic structure.[27,41–44] The distorted MoO_6 octahedra contain edge-sharing zigzag rows along the [001] direction, corner-sharing rows along the [100] direction, and are held together by weak van der Waals' forces in the vertical [010] direction. The crystal structures have three different types of oxygen atoms, terminal O_t, asymmetric O_a and symmetrically bridging O_s. The O_t is along the [010] direction and only bonds to one Mo atom. The O_a bonds to two Mo atoms with different bond lengths along the [100] direction and the O_s bonds to three Mo atoms with two symmetric horizontal bonds and one vertical bond along the [001] direction. In our design, we define crystal direction [100] and [001] as x- and y-direction, respectively, in the Cartesian coordinate system. The equilibrium bond distance and atomic spacings significantly influence the properties of α-MoO_3 and can result in unique anisotropic optical properties. From the measurement of optical spectra of α-MoO_3 cavities, we fit the oscillators of optical spectra to achieve a complex dielectric function in the form of

$$\varepsilon(\omega) = \varepsilon_\infty + \sum_i \frac{\omega_{pi}^2}{\omega_{oi}^2 - \omega^2 - i\gamma_i\omega} \quad (1)$$

where i is the total number of oscillators, ε_∞, ω_{pi}, ω_{oi}, and γ_i are respectively the high frequency dielectric constant, the plasma frequency, the eigenfrequency, and the scattering rate of the ith Lorentz oscillator. Using Kramers–Kronig constrained variational analysis,[45] we determine the complex refractive index of α-MoO_3. The parameters used in Equation (1) are listed in Table S1, Supporting Information. Figure 1c and Figure S1, Supporting Information, show the complex refractive index and dielectric function of α-MoO_3. In addition to the remarkable anisotropic optical properties of α-MoO_3 in the infrared regime,[26–28] interesting optical anisotropy is observed in the

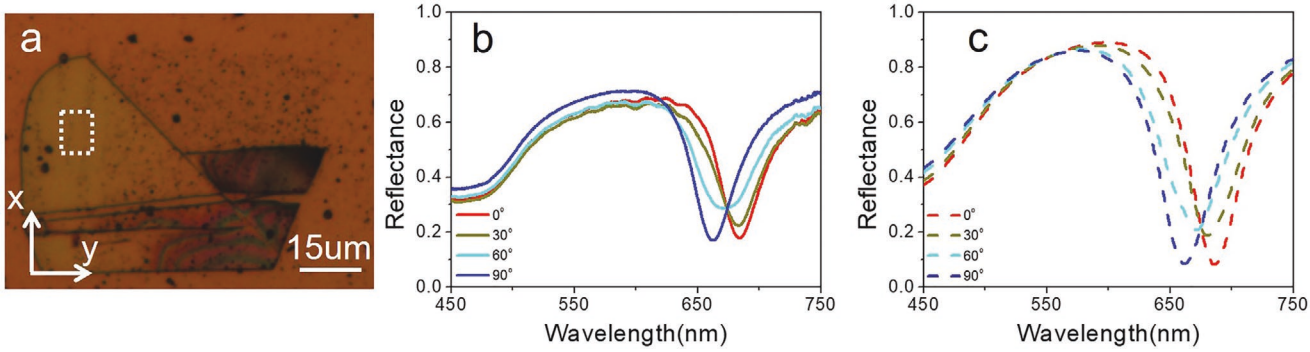

Figure 2. a) Optical image of α-MoO_3 polarization reflector with thickness $t = 30$ nm, $h = 80$ nm, and $b = 150$ nm. White dashed square represent the measured area. b) Measured and c) simulated reflectance spectra for α-MoO_3 polarization reflector. The incident light is linearly polarized in directions ranging from the x to y crystal axes (0° to 90°) in 30° steps.

visible frequency range(450–750 nm) between x and y polarization, as well. Compared to the other birefringent materials, such as BP[17] and $CaCO_3$[46] as shown in Figure S2, Supporting Information, the complex refractive index of α-MoO_3 represents good trade-off between high index contrast and low loss.

To further explore the properties of α-MoO_3 in the visible regime, we design a polarization-sensitive reflection filter. **Figure 2**a shows the optical image of a cavity containing α-MoO_3 (≈80 nm) fully encapsulated on top and bottom by Au film. We intentionally chose optically thick (b = 150 nm) Au as the bottom metal layer to minimize the transmission. And the top Au film is set to be $t = 30$ nm to balance the light penetration into the planar nanocavity with the material losses. To experimentally verify the polarization-dependent function of the device, we performed polarization-dependent reflectance measurements on a designed α-MoO_3 cavity, as shown in Figure 2b. The reflectance spectrum with normally incident light polarized along x-axis (defined as 0° polarization) of α-MoO_3 crystal has a resonance peak wavelength at 684 nm due to the resonance of the FP cavity related to the thickness of the α-MoO_3. Since the crystal structure of α-MoO_3 is sensitive to the polarization of the incident light, the peak wavelength of reflectance spectrum shifts to 662 nm when the light polarized along y-axis (defined as 90° polarization). One can see the continuous shifting of the peak wavelength of reflectance spectra with the polarization angle changing from the x- to y-direction as shown in Figure S3, Supporting Information. Moreover, by tuning the thickness of α-MoO_3, the polarization device could work across the whole visible range as shown in Figure S4, Supporting Information.

The Transfer-matrix method (TMM) is a general method used in optics to analyze the propagation of electromagnetic waves through layered media.[47] Utilizing TMM, we calculate the expected reflectance spectra by fitting complex reflective index of α-MoO_3 and Lorentz–Drude model of Au[48] in the visible range. The reflectance spectra for α-MoO_3 cavities with varying polarization angles are plotted in Figure 2c. The overall sharp and the resonance peak wavelength match quite well with the measured ones. The slight discrepancies in overall intensity can be attributed to surface roughness of stemming from the α-MoO_3 flake, as shown in Figure S5a, Supporting Information.

When the thickness of the bottom metallic film is reduced, the incident light can propagate through the α-MoO_3 cavities, which allows the α-MoO_3 cavities to act as color filters. We choose Ag as the metallic film on top and bottom for lower optical losses and higher quality factors. Moreover, thinner Ag layers lead to higher transmission. However, the experimental procedure, in this case, sets a limit on the minimal film thickness of Ag. Namely, Ag layers thinner than 20 nm do not form continuous layers and tended to delaminate during the α-MoO_3 transfer process. As such, the thicknesses of the top and bottom Ag are set to 20 and 30 nm, respectively. **Figure 3**a,b shows the optical image of α-MoO_3 polarization color filter under transmittance mode for 0° polarization and 90° polarization, respectively. Since the α-MoO_3 surface is not planar, multiple colors appear on the optical image. Thus, we choose a small area for the following measurement marked as white dash line square in Figure 3a,b. In the square, the thickness of the α-MoO_3 is approximately 260 nm. Measured transmittance spectra for both x and y polarizations in the square area marked on flake images are plotted in Figure 3c. As the polarization changes, the color in the square shows chartreuse (peak wavelength λ_p = 573 nm) on 0° polarization (x) and turns to green (peak wavelength λ_p = 551 nm) on 90° polarization (y). Based on the principles of the FP cavity, the thickness of dielectric layer is an important factor determining the resonance peak wavelength. The polarization color filter could be designed to work across the visible range by tuning the thickness of α-MoO_3. As an example, another α-MoO_3 polarization color filter is designed and realized with orange (λ_p = 599 nm) in the measured square area on 0° polarization and green (λ_p = 574 nm) on 90° polarization, as shown in Figure S6, Supporting Information.

To verify the fitting of the refractive index of α-MoO_3 in the visible range, we fabricated an Ag/α-MoO_3/Ag cavity with several transferred α-MoO_3 flakes whose thicknesses vary from 300 to 500 nm. In this FP structure, the thicknesses of top and bottom Ag layers are set to $t = 20$ nm and $b = 20$ nm. **Figure 4**a,c shows the optical image in transmission-mode on x polarization and y polarization. Transmittance spectra can be calculated using TMM by the fitting refractive index of α-MoO_3 and the complex refractive index of Lorentz–Drude model of Ag.[44] Figure 4b,d show the plots of transmittance spectra as a

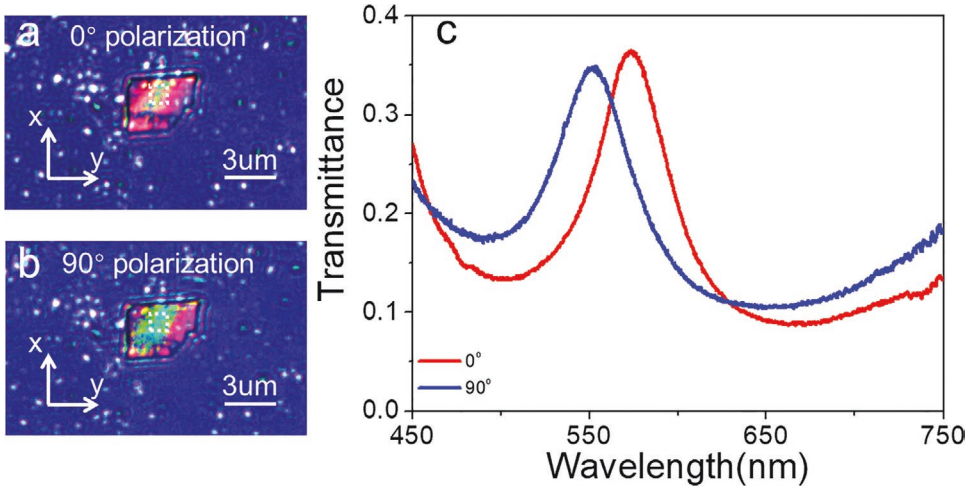

Figure 3. Optical image of α-MoO_3 polarization color filter with thickness t = 20 nm, h = 290 nm, and b = 20 nm for a) 0° polarization and b) 90° incident polarization. White dashed squares represent the measured area. The color turns from chartreuse to green when the linear polarization angle changes from 0° to 90°. c) Corresponding transmittance spectrum of α-MoO_3 polarization color filter.

function of α-MoO_3 thickness and the wavelength on x and y polarization, respectively. One can clearly see that the region of highest intensity in the visible regime changes from magenta to violet when the incident light polarization is switched from x polarization to y polarization owing to anisotropic optical properties of α-MoO_3, which can be represented as a blueshift in transmittance spectra as shown in Figure 4b,d. In FP cavities, free spectral range (FSR) $\Delta\lambda$, which is the wavelength separation between adjacent transmittance peaks, is given by:

$$\Delta\lambda = \frac{\lambda_0^2}{2n_g h\cos\theta + \lambda_0} \tag{2}$$

where λ_0 is the central wavelength of the nearest transmittance peak wavelength, n_g is the effective group refractive index, and

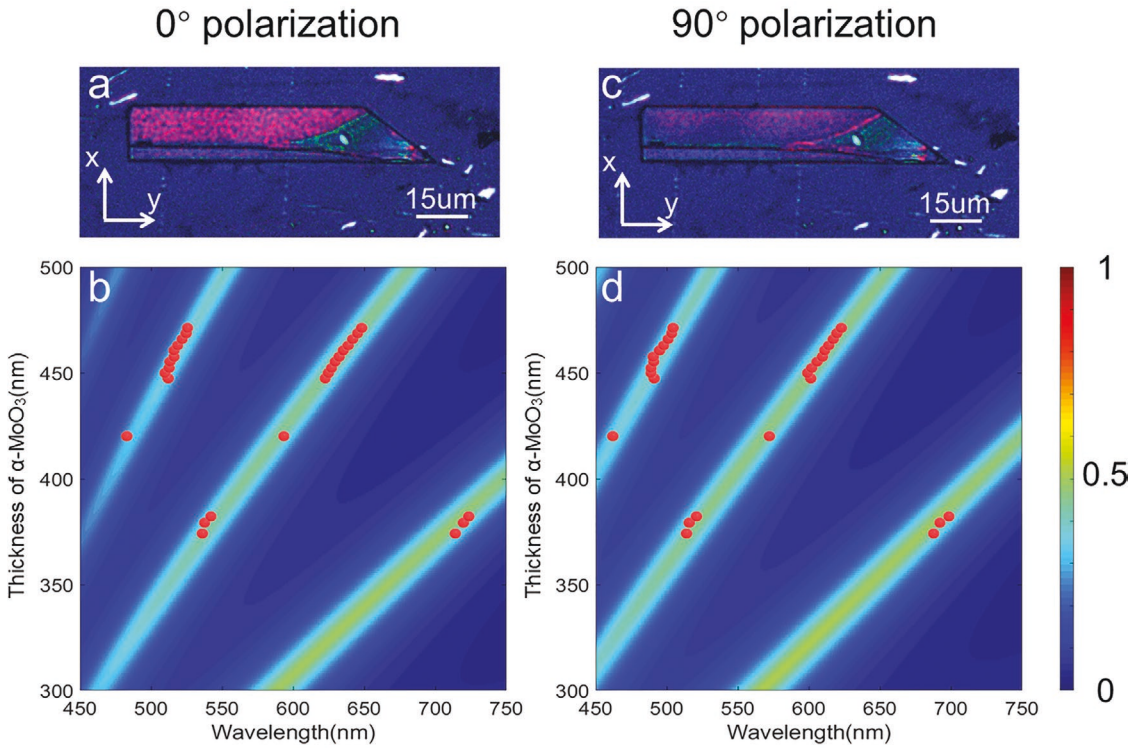

Figure 4. Optical image of α-MoO_3 polarization color filter with thickness t = 20 nm, b = 20 nm and h between 300 and 500 nm under a) x-polarized and c) y-polarized illumination. Transmittance spectrum plotted as a function of wavelength and thickness of α-MoO_3 for incident b) x polarization and d) y polarization. The red spheres indicate the peak wavelengths of experimental results extracted from corresponding mapping experiment of several α-MoO_3 polarization color filters.

h is the thickness of α-MoO_3, θ is the angle of the incident light which is 0° as normally incident.

Along with the increasing of the thickness of α-MoO_3, the decrease of FSR leads to the emergence of multiple resonance peaks in the visible range. Moreover, we mapped the intensity of the transmittance spectra on both x polarization and y polarization. The extracted peak wavelengths from corresponding experimental mapping measurements vary with thickness of α-MoO_3 (red circles in Figure 4b,d) are overlaid on the simulated transmittance spectra and matched well with the multiple resonance peaks. There is little deviation of the extracted peak wavelengths compared to the simulated resonance peaks as a result of the unevenness of the α-MoO_3 surface as shown in Figure S5b, Supporting Information. Furthermore, if the angle of the incident light is increased, the resonance peaks experience blue shift. This behavior is expected which results from the the FP condition,

$$k_z = \frac{2\pi n}{\lambda}\cos\theta = \frac{1}{h}(m\pi - \Delta\varphi), m = 0,1,2,3,\ldots \quad (3)$$

where k_z, λ, n, h, and $\Delta\varphi$ are respectively the momentum in the optical path (surface normal), resonance wavelength, refractive index of α-MoO_3, thickness of α-MoO_3 and the phase picked up in the top and bottom interfaces of α-MoO_3. Equation (3) dictates that increasing the incidence angle should be balanced with smaller λ, hence shorter resonance wavelength is expected. Compared to the normal incident light, the intensity of reflectance spectra decreases as the incidence angle increases, which leads to a higher intensity of transmittance spectra as shown with simulations in Figure S7, Supporting Information.

3. Conclusion

In conclusion, we have studied the anisotropic optical properties of 2D vdW material α-MoO_3 in the visible frequency, which can be widely applied to polarization angle-dependent photonic devices including polarization reflectors and polarization color filters. We proposed and realized a polarization reflector based on the FP cavity with α-MoO_3 in the visible frequency range with continuous polarization dependence. Moreover, we fabricated polarization color filters with α-MoO_3 after constructing leaking mode nanocavity. By tuning the thickness of α-MoO_3, the polarization color filters can work across the entire visible range. We experimentally demonstrated 22 and 25 nm peak position tunability with incidence polarization, for reflection and transmission mode color filters, respectively. No extra device is needed to achieve polarization dependence properties since the anisotropic optical properties of the proposed devices stem from the inherent anisotropic crystal structure of α-MoO_3. Such devices based on 2D vdW α-MoO_3 or other potentially 2D vdW materials[17–19,31,32] can enable polarization sensitivity without complex nanofabrication and provide great flexibility and high throughput manufacturing, which paves the way to more versatile metasurfaces and novel integrated optical devices beyond conventional materials and approaches.

4. Experimental Section

Fabrication: The multilayer FP structure was fabricated using physical vapor deposition (PVD) techniques. Au and Ag for all the samples were deposited on quartz substrates using AJA eBeam Evaporator system and the base and deposition pressures were respectively 9×10^{-7} and 3×10^{-6} Torr. The deposition rate was 0.5 nm s^{-1}.

MoO_3 Growth and Flake Transfer: MoO_3 flakes were grown using low pressure physical vapor deposition. For this process, 50 mg of MoO_3 (Sigma-Aldrich) powder was spread evenly within an alumina boat. This boat was placed within a 1 in. diameter quartz tube and at the center of a small Lindberg tube furnace. A 4 in. × 1 in. rectangular piece of SiO_2/Si wafer (300 nm oxide thickness) was placed face-up downstream in a colder zone of the furnace. These pieces were suspended on top of an alumina boat and were located roughly 4 cm from the center region. The pressure was maintained at 2.8 Torr with a carrier gas of O_2 at a flow rate of 25 sccm. The center of the furnace was then heated to 675 °C over a period of 25 min and then to 700 °C over a period of 5 min. Upon reaching 700 °C, the furnace was immediately opened, thereby quenching the deposition. The as-grown flakes were then mechanically exfoliated using Scotch tape and transferred onto the substrates of interest.

Characterization: For the measurement of the samples, an inverted microscope system was used. The system was established up with a Nikon TI inverted microscope equipped with an Andor Actor spectrometer consisting electron multiplication charge-coupled device (EM-CCD) camera. A broadband halogen lamp with a linear polarizer was used to generate polarize broadband illumination. The reflected and transmitted light was collected by a 50× Nikon microscope objective lens.

Supporting Information

Supporting Information is available from the Wiley Online Library or from the author.

Acknowledgements

K.A. acknowledges support from the Office of Naval Research Young Investigator Program (ONR-YIP) Award (N00014-17-1-2425). The program manager is Brian Bennett. K.A. and V.P.D. acknowledge partial support from the Air Force Office of Scientific Research under Award Number FA9550-17-1-0348. This work was supported by the National Science Foundation under Grant Nos. DMR-1507810 and DMR-1929356. This work made use of the EPIC, Keck-II, SPID, and Northwestern University Micro/Nano Fabrication Facility (NUFAB) facilities of Northwestern University's NUANCE Center, which received support from the Soft and Hybrid Nanotechnology Experimental (SHyNE) Resource (NSF ECCS-1542205); the MRSEC program (NSF DMR-1720319) at the Materials Research Center; the International Institute for Nanotechnology (IIN); the Keck Foundation; and the State of Illinois, through the IIN. C.W. acknowledges support by China Scholarship Council (CSC). A.A.M. gratefully acknowledges support from the Ryan Fellowship and the IIN at Northwestern University.

Conflict of Interest

The authors declare no conflict of interest.

Keywords

α-MoO_3, metal–insulator–metal, polarization color filters, polarization reflectors

Received: January 15, 2020
Revised: February 29, 2020
Published online:

[1] C. Helgert, C. Menzel, C. Rockstuhl, E. Pshenay-Severin, E. B. Kley, A. Chipouline, A. Tunnermann, F. Lederer, T. Pertsch, *Opt. Lett.* **2009**, *34*, 704.
[2] X. Xiong, Z. H. Xue, C. Meng, S. C. Jiang, Y. H. Hu, R. W. Peng, M. Wang, *Phys. Rev. B* **2013**, *88*, 115105.
[3] L. H. Nicholls, F. J. Rodriguez-Fortuno, M. E. Nasir, R. M. Cordova-Castro, N. Olivier, G. A. Wurtz, A. V. Zayats, *Nat. Photonics* **2017**, *11*, 628.
[4] L. Q. Cong, W. Cao, X. Q. Zhang, Z. Tian, J. Q. Gu, R. Singh, J. G. Han, W. L. Zhang, *Appl. Phys. Lett.* **2013**, *103*, 171107.
[5] X. Ling, S. X. Huang, E. H. Hasdeo, L. B. Liang, W. M. Parkin, Y. Tatsumi, A. R. T. Nugraha, A. A. Puretzky, P. M. Das, B. G. Sumpter, D. B. Geohegan, J. Kong, R. Saito, M. Drndic, V. Meunier, M. S. Dresselhaus, *Nano Lett.* **2016**, *16*, 2260.
[6] Z. Z. Liu, S. A. Wells, S. Butun, E. Palacios, M. C. Hersam, K. Aydin, *Nanotechnology* **2018**, *29*, 285202.
[7] S. Jahani, Z. Jacob, *Nat. Nanotechnol.* **2016**, *11*, 23.
[8] O. Takayama, A. A. Bogdanov, A. V. Lavrinenko, *J. Phys.: Condens. Matter* **2017**, *29*, 463001.
[9] K. S. Novoselov, A. Mishchenko, A. Carvalho, A. H. C. Neto, *Science* **2016**, *353*, aac9439.
[10] K. S. Novoselov, D. Jiang, F. Schedin, T. J. Booth, V. V. Khotkevich, S. V. Morozov, A. K. Geim, *Proc. Natl. Acad. Sci. U. S. A.* **2005**, *102*, 10451.
[11] S. X. Yang, Y. H. Yang, M. H. Wu, C. G. Hu, W. F. Shen, Y. J. Gong, L. Huang, C. B. Jiang, Y. Z. Zhang, P. M. Ajayan, *Adv. Funct. Mater.* **2018**, *28*, 1707379.
[12] J. S. Qiao, X. H. Kong, Z. X. Hu, F. Yang, W. Ji, *Nat. Commun.* **2014**, *5*, 4475.
[13] H. T. Yuan, X. G. Liu, F. Afshinmanesh, W. Li, G. Xu, J. Sun, B. Lian, A. G. Curto, G. J. Ye, Y. Hikita, Z. X. Shen, S. C. Zhang, X. H. Chen, M. Brongersma, H. Y. Hwang, Y. Cui, *Nat. Nanotechnol.* **2015**, *10*, 707.
[14] X. S. Li, W. W. Cai, J. H. An, S. Kim, J. Nah, D. X. Yang, R. Piner, A. Velamakanni, I. Jung, E. Tutuc, S. K. Banerjee, L. Colombo, R. S. Ruoff, *Science* **2009**, *324*, 1312.
[15] Z. Z. Liu, K. Aydin, *Nano Lett.* **2016**, *16*, 3457.
[16] X. L. Song, Z. H. Liu, Y. J. Xiang, K. Aydin, *Opt. Express* **2018**, *26*, 5469.
[17] N. Mao, J. Tang, L. Xie, J. Wu, B. Han, J. Lin, S. Deng, W. Ji, H. Xu, K. Liu, L. Tong, J. Zhang, *J. Am. Chem. Soc.* **2016**, *138*, 300.
[18] S. X. Huang, Y. Tatsumi, X. Ling, H. H. Guo, Z. Q. Wang, G. Watson, A. A. Puretzky, D. B. Geohegan, J. Kong, J. Li, T. Yang, R. Saito, M. S. Dresselhaus, *ACS Nano* **2016**, *10*, 8964.
[19] X. L. Song, Z. Z. Liu, J. Scheuer, Y. J. Xiang, K. Aydin, *J. Phys. D: Appl. Phys.* **2019**, *52*, 164002.
[20] G. S. Deng, X. L. Song, S. A. Dereshgi, H. Q. Xu, K. Aydin, *Opt. Express* **2019**, *27*, 23576.
[21] K. S. Novoselov, A. K. Geim, S. V. Morozov, D. Jiang, Y. Zhang, S. V. Dubonos, I. V. Grigorieva, A. A. Firsov, *Science* **2004**, *306*, 666.
[22] E. F. Liu, Y. J. Fu, Y. J. Wang, Y. Q. Feng, H. M. Liu, X. G. Wan, W. Zhou, B. G. Wang, L. B. Shao, C. H. Ho, Y. S. Huang, Z. Y. Cao, L. G. Wang, A. D. Li, J. W. Zeng, F. Q. Song, X. R. Wang, Y. Shi, H. T. Yuan, H. Y. Hwang, Y. Cui, F. Miao, D. Y. Xing, *Nat. Commun.* **2015**, *6*, 6991.
[23] H. Yang, H. Jussila, A. Autere, H. P. Komsa, G. J. Ye, X. H. Chen, T. Hasan, Z. P. Sun, *ACS Photonics* **2017**, *4*, 3023.
[24] M. Q. Huang, M. L. Wang, C. Chen, Z. W. Ma, X. F. Li, J. B. Han, Y. Q. Wu, *Adv. Mater.* **2016**, *28*, 3481.
[25] S. X. Yang, Y. Liu, M. H. Wu, L. D. Zhao, Z. Y. Lin, H. C. Cheng, Y. L. Wang, C. B. Jiang, S. H. Wei, L. Huang, Y. Huang, X. F. Duan, *Nano Res.* **2018**, *11*, 554.
[26] Z. B. Zheng, J. N. Chen, Y. Wang, X. M. Wang, X. B. Chen, P. Y. Liu, J. B. Xu, W. G. Xie, H. J. Chen, S. Z. Deng, N. S. Xu, *Adv. Mater.* **2018**, *30*, 1705318.
[27] W. L. Ma, P. Alonso-Gonzalez, S. J. Li, A. Y. Nikitin, J. Yuan, J. Martin-Sanchez, J. Taboada-Gutierrez, I. Amenabar, P. N. Li, S. Velez, C. Tollan, Z. G. Dai, Y. P. Zhang, S. Sriram, K. Kalantar-Zadeh, S. T. Lee, R. Hillenbrand, Q. L. Bao, *Nature* **2018**, *562*, 557.
[28] Z. B. Zheng, N. S. Xu, S. L. Oscurato, M. Tamagnone, F. S. Sun, Y. Z. Jiang, Y. L. Ke, J. N. Chen, W. C. Huang, W. L. Wilson, A. Ambrosio, S. Z. Deng, H. J. Chen, *Sci. Adv.* **2019**, *5*, eaav8690.
[29] M. Tamagnone, K. Chaudhary, A. Zhu, M. Meretska, J. Li, J. H. Edgar, A. Ambrosio, F. Capasso, *arXiv:1905.02177*, **2019**.
[30] F. X. Ji, X. P. Ren, X. Y. Zheng, Y. C. Liu, L. Q. Pang, J. X. Jiang, S. Z. Liu, *Nanoscale* **2016**, *8*, 8696.
[31] R. S. Datta, F. Haque, M. Mohiuddin, B. J. Carey, N. Syed, A. Zavabeti, B. Zhang, H. Khan, K. J. Berean, J. Z. Ou, N. Mahmood, T. Daeneke, K. Kalantar-zadeh, *J. Mater. Chem. A* **2017**, *5*, 24223.
[32] B. Y. Zhang, A. Zavabeti, A. F. Chrimes, F. Haque, L. A. O'Dell, H. Khan, N. Syed, R. Datta, Y. Wang, A. S. R. Chesman, T. Daeneke, K. Kalantar-zadeh, J. Z. Ou, *Adv. Funct. Mater.* **2018**, *28*, 1706006.
[33] L. X. Sun, Y. Q. Zhang, Y. J. Wang, Y. Yang, C. L. Zhang, X. Y. Weng, S. W. Zhu, X. C. Yuan, *Nanoscale* **2018**, *10*, 1759.
[34] S. M. Kamali, E. Arbabi, A. Arbabi, A. Faraon, *Nanophotonics* **2018**, *7*, 1041.
[35] Y. Bao, Y. Yu, H. Xu, Q. Lin, Y. Wang, J. Li, Z.-K. Zhou, X.-H. Wang, *Adv. Funct. Mater.* **2018**, *28*, 1805306.
[36] S. Sui, H. Ma, J. Wang, Y. Pang, J. Zhang, S. Qu, *Appl. Phys. A* **2016**, *122*, 28.
[37] C. Zhang, D. Wen, F. Yue, Y. Intaravanne, W. Wang, X. Chen, *Phys. Rev. Appl.* **2018**, *10*, 034028.
[38] Z. M. Yang, Y. M. Zhou, Y. Q. Chen, Y. S. Wang, P. Dai, Z. G. Zhang, H. G. Duan, *Adv. Opt. Mater.* **2016**, *4*, 1196.
[39] K. T. Lee, S. Seo, L. J. Guo, *Adv. Opt. Mater.* **2015**, *3*, 347.
[40] Z. Y. Li, S. Butun, K. Aydin, *ACS Photonics* **2015**, *2*, 183.
[41] I. A. de Castro, R. S. Datta, J. Z. Ou, A. Castellanos-Gomez, S. Sriram, T. Daeneke, K. Kalantar-zadeh, *Adv. Mater.* **2017**, *29*, 1701619.
[42] K. Kalantar-zadeh, J. S. Tang, M. S. Wang, K. L. Wang, A. Shailos, K. Galatsis, R. Kojima, V. Strong, A. Lech, W. Wlodarski, R. B. Kaner, *Nanoscale* **2010**, *2*, 429.
[43] W. G. Xie, M. Z. Su, Z. B. Zheng, Y. Wang, L. Gong, F. Y. Xie, W. H. Zhang, Z. Luo, J. Y. Luo, P. Y. Liu, N. S. Xu, S. Z. Deng, H. J. Chen, J. Chen, *ACS Nano* **2016**, *10*, 1662.
[44] S. Balendhran, J. K. Deng, J. Z. Ou, S. Walia, J. Scott, J. S. Tang, K. L. Wang, M. R. Field, S. Russo, S. Zhuiykov, M. S. Strano, N. Medhekar, S. Sriram, M. Bhaskaran, K. Kalantar-Zadeh, *Adv. Mater.* **2013**, *25*, 109.
[45] A. B. Kuzmenko, *Rev. Sci. Instrum.* **2005**, *76*, 083108.
[46] G. Ghosh, *Opt. Commun.* **1999**, *163*, 95.
[47] M. Born, E. Wolf, *Principles of Optics*, Cambridge University Press, Cambridge **1999**.
[48] A. D. Rakic, A. B. Djurisic, J. M. Elazar, M. L. Majewski, *Appl. Opt.* **1998**, *37*, 5271.